Journal of Saudi Chemical Society (2019) **23**, 546–560

King Saud University

Journal of Saudi Chemical Society

www.ksu.edu.sa
www.sciencedirect.com

ORIGINAL ARTICLE

Synthesis, crystal structure analysis, spectral IR, UV–Vis, NMR assessments, electronic and nonlinear optical properties of potent quinoline based derivatives: Interplay of experimental and DFT study

Muhammad Khalid [a,*], **Malik Aman Ullah** [b], **Muhammad Adeel** [b,*], **Muhammad Usman Khan** [c,*], **Muhammad Nawaz Tahir** [d], **Ataualpa Albert Carmo Braga** [e]

[a] *Department of Chemistry, Khwaja Fareed University of Engineering & Information Technology, Rahim Yar Khan 64200, Pakistan*
[b] *Institute of Chemical Sciences, Gomal University, Dera Ismail Khan 29050, Pakistan*
[c] *Department of Applied Chemistry, Government College University, Faisalabad 38000, Pakistan*
[d] *Department of Physics, University of Sargodha, Sargodha 40100, Pakistan*
[e] *Departamento de Química Fundamental, Instituto de Química, Universidade de São Paulo, Avenida Professor Lineu Prestes, 748, São Paulo 05508-000, Brazil*

Received 23 August 2018; revised 17 September 2018; accepted 26 September 2018
Available online 10 October 2018

KEYWORDS

3-Arylated quinolines;
Suzuki–Miyaura cross-coupling;
Crystal structures;
Spectroscopic data;
Density functional theory;
Nonlinear optical properties

Abstract Quinoline and its derivatives are widely studied by both synthetic and computational chemists due to their exciting perspectives in biological and nonlinear optical (NLO) research. Herein, three novel arylated quinolines: 3-(4-acetylphenyl)quinoline (**1**), 3-(4-(methylthio)phenyl)-quinoline (**2**) and 3-(4-phenoxyphenyl)quinoline (**3**) were synthesized employing Pd catalyzed Suzuki–Miyaura cross-coupling reaction. The chemical structures of all compounds were resolved employing different analytical techniques like ^{1}H-NMR, FT-IR, UV–Vis, EIMS, elemental analysis and finally confirmed by single crystal X-ray diffraction analysis. Synthesized compounds were further subjected to density functional theory (DFT) calculations at B3LYP level of theory in conjunction with 6-311 + G(2d,p) basis set to explore optimized geometry, natural bond orbital (NBO)

* Corresponding authors.
E-mail addresses: khalid@iq.usp.br, muhammad.khalid@kfueit.edu.pk (M. Khalid), adeel.gu@yahoo.com (M. Adeel), usman.chemistry@gmail.com (M. Usman Khan).

Peer review under responsibility of King Saud University.

Production and hosting by Elsevier

https://doi.org/10.1016/j.jscs.2018.09.006

analysis, FT-IR spectroscopic data, frontier molecular orbitals (FMOs) and NLO properties. Overall, a good agreement was found between DFT computed results and corresponding experimental findings. Vertical electronic transition states were computationally calculated using time-dependent DFT (TDDFT) at same B3LYP level of theory and 6-311 + G(2d,p) basis set combination. NBO calculations indicated the occurrence of intra-molecular charge transfer in synthesized compounds, hence enormous molecular stability owing to hyperconjugative interactions. Energy of FMOs was used to calculate the global reactivity descriptors which indicated that synthesized molecules are chemically hard compounds with greater kinetic stability and electron donating capability. NLO properties were found to be in the range 1830–2960 a.u and order of **2** > **1** > 3. Urea molecule comparative analysis and two-state model confirmed that synthesized molecules are excellent NLO candidates and may have prospective uses in the technology related applications.

1. Introduction

Numerous pharmacological and chemical properties of quinoline and derivatives of quinoline have attracted the attention of synthetic and biochemists. Due to presence of quinoline subunit in various natural products, this heterocyclic ring has become most important structural motif in medicinal chemistry. Natural products like numerous alkaloids contain quinoline subunit. Compounds with quinoline motifs have a variety of chemotherapeutic activities, especially antibacterial [1], antimalarial [2], antifungal [3], anticancer [4], antileishmanial [5], antitumor [6–8], anti-diabetes [9], immunosuppressive [10,11], antiviral [12], anti-inflammatory [13], HIV-1integrase inhibitory [14], anti-asthma [15], analgesia, vasorelaxing [16], antiplasmodial [17], anticonvulsant and antihypertensive effects [18]. Production of diversified flavoring agents, fungicides, biocides, numerous rubber chemicals and synthetic alkaloids is dependent on derivatives of quinoline [19]. Nano and meso structures of derivatives of quinoline are used in enhancement of electronic and photonic properties [20]. Derivatives of quinolines have found their applications as solvents for terpenes and resins, polymers, catalysts, preservatives and corrosion inhibitors. Besides this, quinoline derivatives are also employed in coatings. Quinoline cores are found in numerous organic compounds such as chemotherapeutic agents, analytical reagents and alkaloids.

Another important area of research is nonlinear optics (NLO) in which quinoline based derivatives are extensively studied by both experimental and theoretical communities due to their low dielectric constants, ultrafast and broadband-electronic responses considered in promising optoelectronic technologies [21–23]. Owing to their countless biological and NLO applications, the syntheses of quinolines have been a subject of great focus in organic synthetic chemistry. Herein, by this research study, we are reporting three new 3-arylated quinolines. This work is an extension to our ongoing research on 3-arylated pyridines. Most recently, we have reported crystal structure data, solubility studies and medicinal importance of this type of compounds [24–26]. In order to broaden the scope of investigations on structure of 3-arylated quinolines and having comparative study background of both synthetic as well as computational studies [27–33], herein we report the synthesis of novel 3-arylated quinoline in excellent yield employing Pd catalyzed Suzuki–Miyaura cross-coupling reaction (Scheme 1) namely; 3-(4-acetylphenyl) quinoline (**1**), 3-(4-(methylthio) phenyl) quinoline (**2**) and 3-(4-phenoxyphenyl) quinoline (**3**). The synthetic, crystal structure analysis, spectroscopic studies and computational investigations of **1**, **2** and **3** are missing as per available current literature. Therefore, **1**, **2** and **3** have been subjected to XRD, ^{1}H-NMR, FT-IR, EIMS, elemental analysis and UV–Vis assessments. DFT calculations have been performed to elucidate the natural bond orbital (NBO) analysis, frontier molecular orbital (FMO) analysis, global reactivity parameters including softness, hardness, ionization potential, electron affinity, electrophilicity index, electron donating as well as accepting capabilities and NLO properties of investigated compounds **1**, **2** and **3**.

2. Experimental section

2.1. Material and methods

We initially tested the reaction of phenylboronic acid (0.529 mmol) with 3-bromoquinoline (0.480 mmol) as a model reaction to establish optimal conditions for cross-coupling using moderately polar to polar solvents, mild to strong bases and diversified Pd catalyst. This coupling reaction was performed in a screw capped pressure tube under dry N_2 gas as an inert atmosphere to avoid oxidation of the Pd(0) catalyst by atmospheric O_2 (Oxygen).

First of all, the reaction was carried out using moderately polar to polar solvents such as THF, toluene, MeOH, dioxane and DMF. First catalyst of choice was $Pd(OAc)_2$ at the boiling temperature of the solvent. Initially, the reaction was tested in

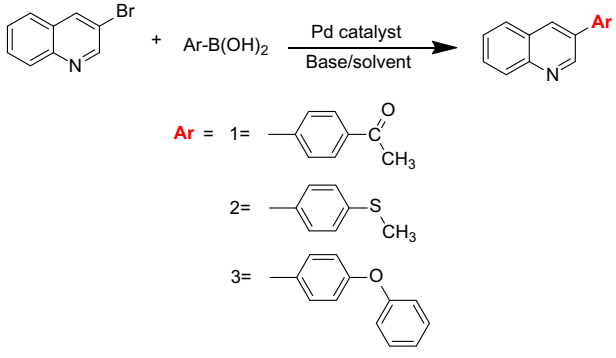

Scheme 1 Schematic representation for the synthesis of **1–3**.

Table 1 Effect of moderately polar to polar solvents.

Entry	Solvent	Catalyst	Base	Temp (°C)	Yield (%)
1	MeOH	$Pd(OAc)_2$	K_2CO_3	65	27
2	THF	$Pd(OAc)_2$	K_2CO_3	66	32
3	Toluene	$Pd(OAc)_2$	K_2CO_3	110	31
4	Dioxane	$Pd(OAc)_2$	K_2CO_3	101	37
5	DMF	$Pd(OAc)_2$	K_2CO_3	153	35

Table 2 Effect of mild to strong bases.

Entry	Solvent	Catalyst	Base	Temperature	Yield (%)
1	Dioxane	$Pd(OAc)_2$	K_2CO_3	100 °C	37
2	Dioxane	$Pd(OAc)_2$	NaOH	100 °C	25
3	Dioxane	$Pd(OAc)_2$	Cs_2CO_3	100 °C	22
4	Dioxane	$Pd(OAc)_2$	K_3PO_4	100 °C	42
5	Dioxane	$Pd(OAc)_2$	Na_2CO_3	100 °C	31

Table 3 Effect of different Pd catalysts.

Entry	Solvent	Catalyst	Base	Temperature	Yield (%)
1	Dioxane	$Pd(OAc)_2$	K_3PO_4	100 °C	42
2	Dioxane	$Pd(PPh_3)_4$	K_3PO_4	100 °C	87
3	Dioxane	$PdCl_2$	K_3PO_4	100 °C	67
4	Dioxane	$Pd_2(dba)_3$	K_3PO_4	100 °C	54

1 ml of H_2O using K_2CO_3 as a base. Under the above conditions, dioxane and DMF proved to be the best solvent (Table 1). However, in order to increase the yield, several mild to strong bases were tested; such as K_2CO_3, Na_2CO_3, Cs_2CO_3, K_3PO_4 and NaOH and dioxane as solvent and $Pd(OAc)_2$ as catalyst at 100 °C. K_3PO_4 was proved to be a good base compared to other bases, other bases had given disappointing results (Table 2). Main focus of this reaction was to select suitable Pd catalyst which must produce high yields. Experimental facts showed that $Pd(PPh_3)_4$ was the best catalyst for this reaction, while other catalyst like $Pd_2(dba)_3$, $Pd(OAc)_2$ and $PdCl_2$ showed poor catalytic activity as compared to $Pd(PPh_3)_4$ at 100 °C with dioxane as solvent (Table 3).

Simple phenylboronic acid (63 mg, 0.519 mmol) coupling with 3-bromoquinoline (0.479 mmol) was chosen as test reaction in 3.5 ml of dioxane as solvent, Pd(PPh3)$_4$ (1.5 mol %, 8.29 mg) and suitable base like K_3PO_4 (149 mg, at 90–100 °C, 0.719 mmol) and most importantly addition of 1–1.5 ml of H_2O is good for salvation of base; which in turn enhance reactivity of reaction. To the best of our knowledge on the bases of experimental facts, we can say that in the case under study, the best suitable conditions are $Pd(PPh_3)_4$, dioxane, K_3PO_4, 90–100 °C and 1–1.5 ml of H_2O.

2.2. Computational procedure

Herein, DFT [34–36] employing Gaussian 09 program package [37] was used to perform complete quantum chemical calculations. The initial geometry for **1**, **2** and **3** was regained from the XRD driven crystal structures. B3LYP level of theory and 6-311 + G(2d,p) basis set combination in gas phase without symmetry restrictions was used to perform complete optimization of **1**, **2** and **3**. Stability of optimized geometries was confirmed by performing frequency analysis at same DFT/B3LYP/6-311 + G(2d,p) functional. Among all calculated frequencies, lack of negative eigen value points out the optimized geometries at real positive and are corresponding to true minimum in the potential energy surface. NBO analysis was also carried out at same level of theory and basis set using Gaussian 09 embedded NBO 3.1 program package. NLO and FMO analysis were performed at B3LYP/6-311 + G(2d,p) level of theory. UV–Vis spectral analysis was exercised to determine the photophysical properties of **1**, **2** and **3** using TDDFT at B3LYP level of theory in conjunction with 6–311 + G(2d,p) basis set. Gauss View 5.0 [38] was used to organize the input files. Output files results were interpreted using Avogadro [39], Chem Craft [40] and Gauss View programs.

3. Results and discussion

3.1. Synthesis of 3-(4-acetylphenyl) quinoline (*1*)

Starting with 3-bromoquinoline(100 mg, 0.4806 mmol),4-acetylphenylboronic acid (86 mg, 0.5287 mmol), Pd (PPh_3)$_4$ (1.5 mol%, 8.33 mg), K_3PO_4 (152 mg, 0.7209 mmol) in dioxane suspension (3 ml), the product was isolated as a light brown crystalline solid (146 mg, 90%).Yield (106 mg, 90%), m.p = 128–130 °C.

^{1}HNMR (400 MHz, DMSO): δ = 2.68 (s, 3H, CH_3), 7.69 (t, 1H, Ar-H), 7.83 (t, 1H, Ar-H), 7.96 (d, 2H, Ar-H), 8.05 (q, 2H, Ar-H), 8.16 (d, 2H, Ar-H), 8.66 (s, 1H, Ar-H), 9.20

(s, 1H, Ar-H). IR (KBr): ύ = 1676 (s), 1598 (m), 1354 (m), 1116 (s), 1267 (m), 825 (s), 752 (m), 584 (m) cm^{-1}. EI-MS (EI, 70 eV): *m/z* (%): 247 (M^+, 100), 232 (25), 204 (15), 176 (11). Elemental analysis: The calculated values are given in parentheses. C: 82.54 (82.59); H: 5.24 (5.28); N: 5.62 (5.66).

*3.2. Synthesis of 3-(4-(methylthio) phenyl) quinoline (**2**)*

Starting with 3-bromoquinoline(100 mg, 0.4806 mmol), 4-(methylsulfanyl) phenylboronic acid (89 mg, 0.5287 mmol), Pd $(PPh_3)_4$ (1.5 mol%, 8.33 mg), K_3PO_4 (152 mg, 0.7209 mmol) in dioxane suspension (3 ml), the productwas isolated as a yellow crystalline solid (146 mg, 90%). (108 mg, 90%), m.p = 90–91 °C. ^{1}HNMR (400 MHz, DMSO): δ = 2.630 (s, 3H, CH_3), 7.581 (d, *J* = 8.2 Hz, 2H, Ar-H), 7.675 (d, *J* = 8.4 Hz, 2H, Ar-H), 7.865 (d, *J* = 8.4 Hz, 1H, Ar-H), 8.126 (d, *J* = 5.2 Hz, 1H, Ar-H), 8.264 (s, 1H, Ar-H), 9.332 (s, 1H, Ar-H). IR (KBr): ύ = 1595(w), 1558 (s), 1489 (m), 1436 (w), 1338 (w), 1098 (m), 1012 (w), 956 (w), 829 (m), 808 (m), 748 (w), 715 (w), 522 (m) cm^{-1}. EI-MS (EI, 70 eV): *m/z* (%): 251 (M^+, 100), 237 (26), 205 (45), 143 (28), 129 (18). Elemental analysis: for $C_{16}H_{13}NS$: The calculated values are given in parentheses. C: 76.45 (76.49); H: 5.13 (5.17); N: 5.53 (5.57).

*3.3. Synthesis of 3-(4-phenoxyphenyl) quinoline (**3**)*

Starting with 3-bromoquinoline (100 mg, 0.4806 mmol), 4-phenoxyphenyl boronic acid (113 mg, 0.5287 mmol), Pd $(PPh_3)_4$ (1.5 mol%, 8.33 mg), K_3PO_4 (152 mg, 0.7209 mmol) in dioxane suspension (3 ml), the productwas isolated as a white crystalline solid (120 mg, 85%), m.p = 124–126 °C. ^{1}HNMR (400 MHz, $CDCl_3$): δ = 7.121–7.158 (m, 5H, Ar-H), 7.348 (t, 1H, Ar-H), 7.539 (t, 1H, Ar-H), 7.644–7.720 (m, 4H, Ar-H), 7.844 (d, *J* = 8.2 Hz, 1H, Ar-H), 8.111 (d, *J* = Hz, 1H, Ar-H), 8.250 (s, 1H, Ar-H), 9.151 (s, 1H, ArH). IR (KBr): ύ = 1558 (s), 1506 (m), 1489 (w), 1220 (m), 1168 (w), 831 (w), 802 (w), 786 (w), 698(w) cm^{-1}. EI-MS (EI, 70 eV): *m/z* (%): 297.2 (M^+, 100), 268 (23), 220 (28), 192 (28), 77 (15). Elemental analysis: for $C_{21}H_{15}NO$: The calculated values are given in parentheses. C: 84.78 (84.84); H: 4.46 (5.05); N: 3.66 (4.71).

4. Structural insight by XRD study

The crystal data, data collection parameters and refinement results of compounds (**1–3**) are summarized in Table 4.

*4.1. Compound (**1**)*

In 3-(4-acetophenyl)quinoline (Fig. 1a), the quinoline group A (C1–C9/N1), benzene ring B (C10–C15) are planar with r. m. s. deviation of 0.0031 and 0.0014 Å, respectively. The dihedral angle between A/B is 6.67 (11)°. The aceto group C (C16/C17/O1) is oriented at a dihedral angle of 7.71 (26)° and 3.15 (28)° with the quinoline and phenyl groups, respectively. There are no significant hydrogen bonds in these molecules.

Table 4 Crystal data and structure refinement parameters for the compounds **1–3**.

Crystal parameters	Compound (1)	Compound (2)	Compound (3)
CCDC	1,863,235	1,863,234	1,863,236
Empirical formula	$C_{17}H_{13}NO$	$C_{16}H_{13}NS$	$C_{21}H_{15}NO$
Formula weight	247.29	251.35	297.35
Wavelength (Å)	0.71073	0.71073	0.71073
Crystal system	Monoclinic	Monoclinic	Monoclinic
Space group	P21/c	P21/c	P21/c
Unit cell dimensions (Å)	a = 15.0073 (19)	a = 9.6909 (6)	a = 11.042 (1)
	b = 5.5014 (7)	b = 5.6435 (3)	b = 11.7744 (8)
	c = 15.712 (2)	c = 23.345 (15) β = 99.673 (2)°	c = 12.2150 (9)
	β = 108.317 (8)°		β = 98.866 (3)°
Volume ($Å^3$)	1231.5 (3)	1258.61 (13)	1569.1 (2)
Z	4	4	4
Density (mg/m^3)	1.334	1.326	1.259
Absorption coefficient (μ) mm^{-1}	0.08	0.24	0.08
F (0 0 0)	520	528	624
Crystal size (mm^3)	0.38 × 0.31 × 0.24	0.32 × 0.26 × 0.16	0.30 × 0.21 × 0.18
Index ranges	$-19 \le h \le 13$	$-11 \le h \le 9$	$-14 \le h \le 13$
	$-7 \le k \le 6$	$-6 \le k \le 6$	$-15 \le k \le 10$
	$-20 \le l \le 20$	$-28 \le l \le 28$	$-12 \le l \le 16$
Reflections collected	10,481	9746	13,316
Independent reflections	2800 [R (int) = 0.044]	2455 [R(int) = 0.033]	3702 [R (int) = 0.032]
Data/restraints/parameters	2800/0/173	2455/0/164	3702/0/208
ɵ range for data collection/°	1.429 to 27.524	1.77 to 26	1.867 to 27.785
Goodness-of-fit on F^2	0.983	1.015	1.00
Final R indexes R [F2 > 2σ (F2)]	R1 = 0.0615,	R1 = 0.0408,	R1 = 0.0469,
	wR2 = 0.1246	wR2 = 0.0925	wR2 = 0.1019
Final R indexes wR2 [all data]	R1 = 0.1460,	R1 = 0.0741,	R1 = 0.0901,
	wR2 = 0.1575	wR2 = 0.1063	wR2 = 0.1217
$\Delta\rho_{max}$, $\Delta\rho_{min}$ (e $Å^{-3}$)	0.19, −0.17	0.17, −0.21	0.13, −0.20

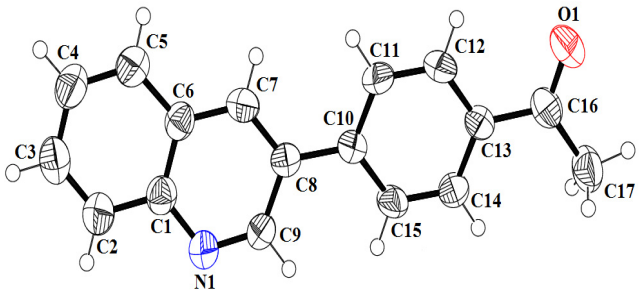

(a) The ORTEP diagram

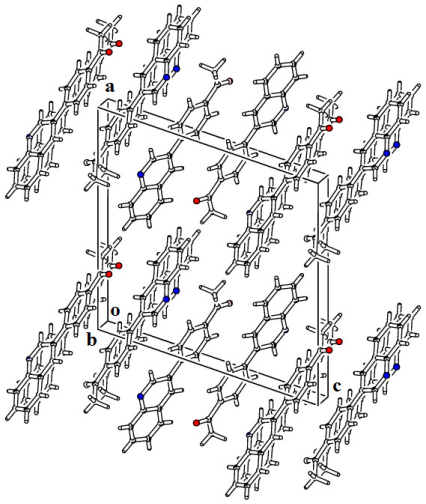

(b) Molecular packing

Fig. 1 (a) ORTEP diagram with thermal ellipsoids drawn at 50% probability level. The H-atoms are drawn as small circles of arbitrary radii. (b) Molecular packing diagram.

The molecules are mainly stabilized due to the Van der Waal's forces. Let the centroids of four six member rings, namely C (N1/C1/C6–C9), D (C1–C6) and E (C10–C15) be Cg1, Cg2 and Cg3, respectively. Then the π-π interaction between $Cg1–Cg^{i}$ [3.1713(9) Å with slippage 4.495 Å] and $Cg2–Cg1^{i}$ [3.1650(9) Å], where the symmetry operations is i = x, 1 − y, z. The packing diagram is given in Fig. 1b.

*4.2. Compound (**2**)*

In 3-[4-(methylsulfanyl)phenyl]quinoline (Fig. 2), the quinoline group A (C1–C9/N1) and phenyl ring B (C10–C15) of 4-(methylsulfanyl)phenyl group are planar with r. m. s. deviation of 0.0162 and 0.0055 Å, respectively. The dihedral angle between A/B is 24.01 (8)°. There exist π-π stacking between the centroids Cg1, Cg2 and Cg3 of the aromatic rings C (N1/C1/C6–C9), D (C1–C6) and E (C10–C15), respectively. The shortest perpendicular distance of 2.7809(8) Å occurs between the centroids $Cg1\ldots Cg2^{i}$ [i = x, 1 + y, z] and largest perpendicular distance of 4.0397(7) Å is between the centroids $Cg1\ldots Cg3^{ii}$ [ii = 2 − x, 1 − y, −z]. The π-π interactions have the major role of stabilizing the molecules.

4.3. Compound (3)

In 3-(4-phenoxyphenyl)quinoline (Fig. 3a), the quinoline group A (C1–C9/N1), benzene ring B (C10–C15) and the attached phenolic group C (O1/C16–C21) are planar with r. m. s. deviation of 0.0100, 0.0061 and 0.0080 Å, respectively. The dihedral angle between A/B, A/C and B/C is 28.23 (6)°, 61.21 (4)° and 78.28 (4)°, respectively. There are no significant hydrogen bonds. The molecules are mainly stabilized due to the Van der Waal's forces. Let the centroids of four six

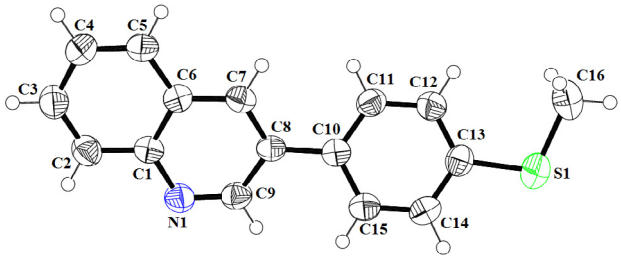

(a) The ORTEP diagram

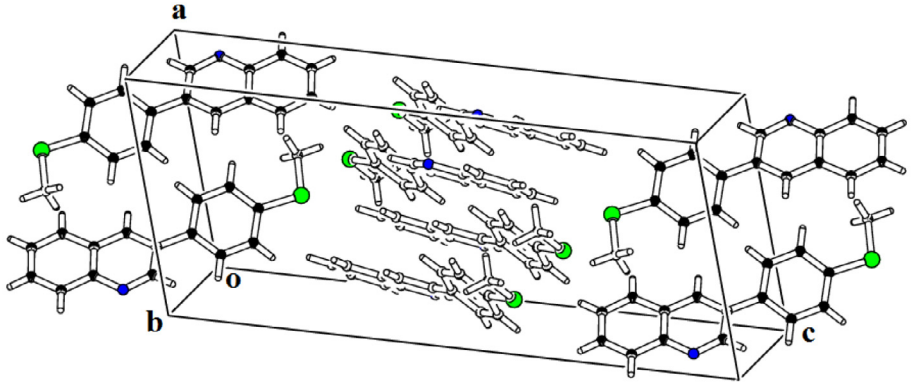

Fig. 2 (a) ORTEP diagram with thermal ellipsoids drawn at 50% probability level. The H-atoms are drawn as small circles of arbitrary radii. (b) Molecular packing diagram.

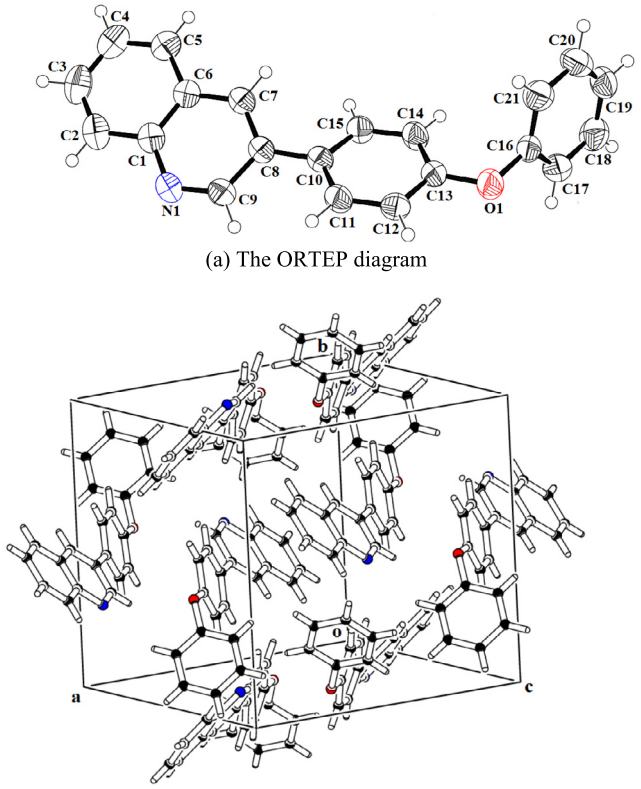

(a) The ORTEP diagram

(b) Molecular packing

Fig. 3 (a) ORTEP diagram with thermal ellipsoids drawn at 50% probability level. The H-atoms are drawn as small circles of arbitrary radii. (b) Molecular packing diagram.

member rings, namely D (N1/C1/C6–C9), E (C1–C6), F (C10–C15) and G (C16–C21) be Cg1, Cg2, Cg3 and Cg4, respectively. Then the π-π interaction between Cg1–Cg^{i} [3.4544(6) Å with slippage 2.843 Å], Cg1–Cg2^{i} [3.4657(7) Å], Cg1–Cg3^{ii} [3.6369(6) Å], Cg2–Cg^{i} [3.4848(6) Å], Cg2–Cg3^{i} [3.3855(6) Å] and Cg4-Cg3^{iii} [3.1836(6) Å] exist, where the symmetry operations are i = 1 − x, 1 − y,1 − z, ii = 1 − x, 1/2 + y, 1/2 − z and iii = −x, 1 − y, −z. The distance given of the second centroid from the first one is perpendicular distance. The packing diagram is given in Fig. 3b.

5. Geometric structures

Complete computational optimization was performed using DFT at B3LYP level of theory in combination with 6-311 + G(2d,p) basis set to calculate to the structural parameters including bond length and bond angle of **1**, **2** and **3**. The DFT calculated structural parameters were compared with the corresponding crystal structure parameters obtained from XRD. Structural parameters of **1**–**3** obtained from DFT and XRD studies have been determined in accordance with the atom numbering scheme of the molecules shown in Scheme 1, Fig. S1 and are depicted in Tables S1–S3 respectively. Results illustrate that the DFT calculated bond lengths and bond angles coincide nicely with corresponding XRD calculated data. The bond lengths in **1**, **2** and **3** are deviated in the range of 0 ± 0.04 Å, 0.05 ± 0.01 Å and 0.25 ± 0.23 Å respectively. Deviation in the bond angles is observed in the range of 2.3° ± 1.8°, 1.0° ± 0.9° and 2.7° ± 1.1° respectively. The DFT calculated C—C bond distance in the benzene ring is found to be in the range of 1.371–1.478 Å in **1**, 1.371–1.775 Å in **2** and 1.371–1.479 Å in **3** which coincides in a good way with their XRD calculated ranges 1.364–1.475 Å, 1.361–1.757 Å and 1.366–1.483 Å respectively. The bond length values of C-N in **1** are measured as 1.363 Å and 1.309 Å for C(1)-N(18) and C(9)-N(18) through DFT that are in good agreement with XRD calculated values 1.363 Å and 1.304 Å. In **2**, C—N bond length value is calculated as 1.363 Å, 1.309 Å through DFT and 1.372 Å, 1.310 Å through XRD for N(2)-C(3) and N(2)-C(11) respectively. Similarly in **3**, DFT calculated C—N bond length is found to be of same values 1.363 Å and 1.309 Å, while XRD calculated vales are observed to be1.375 Å and 1.313 Å for N(2)-C(3) and N(2)-C(11) respectively. The maximum deviation value of bond angle is observed for C(7)-C(8)-C(9) and C(8)-C(9)-N(18) in **1** as 116.9°, 124.9° (DFT) and 114.6°, 126.7° (XRD) respectively. In **2**, bond angles are deviated utmost for N(2)-C(11)-C(10) and C(3)-N(2)-C(11) with value of 118.2°, 125.0° through DFT and 117.3°, 126.0° through XRD respectively. In **3**, maximum deviation in bond angles is calculated to be 120.5°, 125.0° (DFT) and 117.8°, 126.1° (XRD) for C(15)-O(1)-C(18) and N(2)-C(11)-C(10) respectively. Preceding discussion describe good agreement between structural parameters calculated through DFT and XRD studies.

6. Natural bond orbitals (NBO) analysis

NBO analysis is proven as a most reliable method to have orbital level insights on the charge transfer, conjugative interaction, inter- and intra-molecular bonding between the electron rich and electron deficient counterparts [41]. NBO is also helpful in elucidating the steady picture for transfer of charge densities from filled, bonding or donor Lewis-type NBOs to the empty, non bonding or non-Lewis NBOs. The stabilization energy $E^{(2)}$ because of the donor–acceptor interaction can be characterized using second-order perturbation theory. In the NBO analysis, NBO (i) represents donor, NBO (j) represents acceptor and the $E^{(2)}$ means stabilization energy corresponds to the delocalization of electrons between donor and acceptor is relationship as

$$E^{(2)} = q_i \frac{(F_{i,j})^2}{\varepsilon_j - \varepsilon_i} \quad (1)$$

In this equation, q_i represent orbital occupancy, ε_i, ε_j correspond to diagonal NBO Fock matrix elements while $F_{i,j}$ denotes off-diagonal NBO Fock matrix elements respectively. Assuming all these considerations, NBO analysis was carried out for **1**, **2**, **3** at B3LYP level of theory and 6-311 + G(2d, p) basis set combination and results are presented in Tables S4–S6 respectively.

The most credible transitions observed in our studied compounds are: $\pi(C_{17}–C_{19}) \rightarrow \pi^*(C_{16}–H_{24})$ in **1** having stabilization energy vale 21.95 kJ/mol, $\pi(C_{13}–C_{15}) \rightarrow \pi^*(N_2–C_6)$ in **2** with 21.44 kJ/mol stabilization energy value and $\pi(C_{35}–C_{37}) \rightarrow \pi^*(C_8–C_{10})$ transition in **3** with gigantic stabilization energy value found to be 3580.66 kJ/mol. These are the massive stabilization energy values observed in studied compounds. The gigantic stabilization energy value of **3** as compared to **1** and **2** is due to the involvement of intra-

Table 5 Experimental and theoretical vibrational frequencies of **1** at B3LYP/6-311 + G(2d,p) level of theory with proposed assignments.

IR frequency (cm^{-1}) (Exp)	Unscaled frequency (cm^{-1}) (Theo)	I_{IR}	Vibrational assignments
312	302	0.8845	υ (as) C═C─C═C─C_{Ben}
584	583	5.524	υ (as) C═C─C═C─C_{Ben}
752	755	10.30	υ (as) C═C─C═C─C_{Ben} + υ (w) C─H_{Ben}
1267	1265	1.043	υ (δ) C─H_{Ben} + υ (ρ) C─H_{Ben} + υ (as) C═C─C═C─C_{Ben}
1354	1340	9.213	υ (ρ) C─H_{Ben} + υ (as) C═C─C═C─C_{Ben}
1598	1598	1.900	υ (ρ) C─H_{Ben} + υ (as) C═C─C═C─C_{Ben}
1676	1655	0.1848	υ (δ) C─H_{Ben} + υ (as) C═C─C═C─C_{Ben}
	3033	2.8678	υ (s) C─H_{Meth}
	3088	6.636	υ (as) C─H_{Meth}
	3140	14.3728	υ (as) C─H_{Meth}
	3159	0.7228	υ (as) C─H_{Ben}
	3171	7.6891	υ (s + as) C─H_{Ben}
	3174	6.0507	υ (as) C─H_{Ben}
	3175	6.0507	υ (as) C─H_{Ben}
	3184	16.1397	υ (s + as) C─H_{Ben}
	3192	7.7252	υ (s) C─H_{Ben}
	3195	12.8103	υ (s) C─H_{Ben}
	3198	1.9605	υ (s) C─H_{Ben}

υ, stretching; δ, scissoring; ρ, rocking; w, wagging; s, symmetric; as, asymmetric; τ, twisting; Ben, benzene ring; Meth, methyl group; Exp, experimental; Theo, theoretical.

molecular hyper conjugative interactions that originates as a result of extended conjugation present in **3**. The question about the existence of conjugation in the title compounds can be answered with the study of $\pi \rightarrow \pi^*$ interactions which leads to the examination of charge transfer among compounds. Some other transitions observed in **1** representing conjugation are $\pi(C_1–C_{10}) \rightarrow \pi^*(C_6–C_8)$, $\pi(C_1–C_{10}) \rightarrow \pi^*(C_{11}–C_{13})$, $\pi(C_2–C_4) \rightarrow \pi^*(C_1–C_{10})$, $\pi(C_6–C_8) \rightarrow \pi^*(C_1–C_{10})$, $\pi(C_{16}–C_{24}) \rightarrow \pi^*(C_{21}–C_{22})$, $\pi(C_{21}–C_{22}) \rightarrow \pi^*(C_{16}–C_{24})$ and $\pi(C_{26}–C_{27}) \rightarrow \pi^*(C_{26}–O_{32})$ with stabilization energy values found to be 16.22, 18.41, 17.39, 16.33, 19.72, 18.64 and 13.52 kJ/mol respectively. Similarly, transition such as $\pi(C_3–C_{12}) \rightarrow \pi^*(C_{13}–C_{15})$, $\pi(C_4–C_6) \rightarrow \pi^*(C_3–C_{12})$, $\pi(C_8–C_{10}) \rightarrow \pi^*(C_4–C_6)$, $\pi(C_{18}–C_{19}) \rightarrow \pi^*(C_{21}–C_{23})$, $\pi(C_{18}–C_{19}) \rightarrow \pi^*(C_{24}–C_{26})$, $\pi(C_{21}–C_{23}) \rightarrow \pi^*(C_{18}–C_{19})$ and $\pi(C_{24}–C_{26}) \rightarrow \pi^*(C_{21}–C_{23})$ observed in **2** represents conjugation leading to stabilization energy values computed to be 15.11, 12.17, 16.93, 17.72, 21.38, 20.85 and 18.62 kJ/mol respectively. In the same way, transition energy values 157.68, 2707.35, 329.89, 149.82 and 69.32 kJ/mol due to the transitions $\pi(C_6–C_8) \rightarrow \pi^*(C_8–C_{10})$, $\pi(C_{28}–C_{37}) \rightarrow \pi^*(C_8–C_{10})$, $\pi(C_{28}–C_{37}) \rightarrow \pi^*(C_{18}–C_{26})$, $\pi(C_{33}–C_{35}) \rightarrow \pi^*(C_8–C_{10})$ and $\pi(C_{35}–C_{36}) \rightarrow \pi^*(C_8–C_{10})$ respectively describe the presence of conjugation in **3** (see Tables S4–S6). Contrary to $\pi \rightarrow \pi^*$ transitions, $\sigma \rightarrow \sigma^*$ interactions originates due to feeble donor (σ)-acceptor (σ^*) interaction which results in small stabilization energy values. Therefore, small stabilization energy value of 0.50 kJ/mol is observed in **1** due to $\sigma(C_8–H_9) \rightarrow \sigma^*(C_8–H_{10})$ transition. Similar trend is observed in **2** and **3** where $\sigma(S_1–C_{23}) \rightarrow \sigma^*(C_{28}–H_{30})$ and $\sigma(N_2–C_{16}) \rightarrow \sigma^*(C_{13}–C_{15})$ results in small stabilization energy values 0.50 kJ/mol and 0.61 kJ/mol respectively. In addition, some transitions such as $LP(N_{31}) \rightarrow \sigma^*(C_8–H_9)$, $LP(N_2) \rightarrow \sigma^*(C_{15}–C_{16})$ and $LP(O_1) \rightarrow \sigma^*(C_8–C_{10})$ are observed in case of resonance which leads to substantial stabilization energy values 10.04, 10.22 and 198.14 kJ/mol in **1**, **2** and **3** respectively. Above discussion helps make conclusion about the presence of extended conjugation, intramolecular charge transfer and hyperconjugative interactions in studied compounds. In addition, charge transfer character and presence of extended conjugation collectively present a sign of red shift behavior and potential NLO character in studied compounds.

7. FT-IR analysis

Modern vibrational spectroscopy driven molecular vibrations are widely explored by both theoretical as well as experimental communities. Full vibrational analysis including theoretical and experimental infrared calculations was performed to recognize the nature of vibrational modes present in **1**, **2** and **3**. Theoretical vibrational spectra were calculated in gas phase using B3LYP level of theory and 6-311 + G(2d,p) basis set combination. Animation option of Gauss-View was used to assign the vibrational modes present in studied compounds. Most important experimental and theoretical FT-IR results for investigated compounds **1**, **2** and **3** are depicted in Tables 5–7 respectively.

7.1. C–H vibrations

Comparative analysis of computed and experimental vibrational bands of C-H revealed that computed vibrational bands at 755, 1265, 1340, 1598 and 1655 cm^{-1} in **1** are in good agreement with the experimental vibrations bands found at 752, 1267, 1354, 1598 and 1676 cm^{-1} respectively. C-H vibrational bands in **2** computed at 805, 831, 1106, 1495 and 1596 cm^{-1} were strongly supported by experimental bands measured at 810, 829, 1097, 1492 and 1593 respectively. Similar trend is observed in **3** where computed vibrational bands observed at 708, 764, 805, 829, 1168, 1222, 1489, 1496 and 1612 cm^{-1}

Table 6 Experimental and theoretical vibrational frequencies of **2** at B3LYP/6-311 + G(2d,p) level of theory with proposed assignments.

IR frequency (cm^{-1}) (Exp)	Unscaled frequency (cm^{-1}) (Theo)	I_{IR}	Vibrational assignments
746	749	1.052	υ (as) C═C─C═C─C_{Ben}
810	805	7.176	υ (τ) C─H_{Ben}
829	831	29.22	υ (ρ) C─H_{Ben}
1097	1106	79.04	υ (ρ) C─H_{Ben} + υ (as) C═C─C═C─C_{Ben}
1492	1495	7.684	υ (ρ) C─H_{Ben} + υ (as) C═C─C═C─C_{Ben}
1593	1596	5.641	υ (δ) C─H_{Ben} + υ (as) C═C─C═C─C_{Ben}
	3039	22.99	υ (s) C─H_{Meth}
	3120	6.830	υ (as) C─H_{Meth}
	3129	3.218	υ (as) C─H_{Meth}
	3157	0.792	υ (as) C─H_{Ben}
	3161	10.77	υ (s + as) C─H_{Ben}
	3164	6.411	υ (as) C─H_{Ben}
	3169	7.713	υ (s + as) C─H_{Ben}
	3170	5.539	υ (s + as) C─H_{Ben}
	3181	7.432	υ (s) C─H_{Ben}
	3182	17.76	υ (s + as) C─H_{Ben}
	3194	14.49	υ (s) C─H_{Ben}
	3201	6.458	υ (s) C─H_{Ben}

υ, stretching; δ, scissoring; ρ, rocking; w, wagging; s, symmetric; as, asymmetric; τ, twisting; Ben, benzene ring; Meth, methyl group; Exp, experimental; Theo, theoretical.

Table 7 Experimental and theoretical vibrational frequencies of **3** at B3LYP/6-311 + G(2d,p) level of theory with proposed assignments.

IR frequency (cm^{-1}) (Exp)	Unscaled frequency (cm^{-1}) (Theo)	I_{IR}	Vibrational assignments
698	708	37.53	υ (w) C─H_{Ben}
754	764	30.84	υ (w) C─H_{Ben}
786	780	5.178	υ (as) C═C─C═C─C_{Ben}
802	805	2.703	υ (τ) C─H_{Ben}
831	829	1.113	υ (τ) C─H_{Ben}
1168	1168	5.413	υ (δ) C─H_{Ben} + υ (as) C═C─C═C─C_{Ben}
1224	1222	21.99	υ (δ) C─H_{Ben} + υ (as) C═C─C═C─C_{Ben}
1489	1489	1.983	υ (ρ) C─H_{Ben} + υ (as) C═C─C═C─C_{Ben}
1506	1496	17.34	υ (ρ) C─H_{Ben} + υ (as) C═C─C═C─C_{Ben}
1558	1543	137.6	υ (ρ) C─H_{Ben} + υ (as) C═C─C═C─C_{Ben}
	3157	0.576	υ (as) C─H_{Ben}
	3160	10.71	υ (as) C─H_{Ben}
	3165	1.719	υ (as) C─H_{Ben}
	3169	8.657	υ (s + as) C─H_{Ben}
	3172	6.724	υ (as) C─H_{Ben}
	3174	7.317	υ (as) C─H_{Ben}
	3182	17.79	υ (s + as) C─H_{Ben}
	3185	21.41	υ (s + as) C─H_{Ben}
	3193	4.803	υ (s) C─H_{Ben}
	3194	14.36	υ (s) C─H_{Ben}
	3195	2.835	υ (s) C─H_{Ben}
	3198	3.751	υ (s) C─H_{Ben}

υ, stretching; δ, scissoring; ρ, rocking; w, wagging; s, symmetric; as, asymmetric; τ, twisting; Ben, benzene ring; Meth, methyl group; Exp, experimental; Theo, theoretical.

reflects excellent consistency with experimentally measured bands at 698, 764, 802, 831, 1168, 1224, 1489, 1506 and 1558 cm^{-1} respectively.

Furthermore, literature study reveals that aromatic ring and heteroaromatic ring due to structural similarity exhibit C-H stretching vibrations in the ambit of 3100–3000 cm^{-1} [42]. Diverse C-H vibrational bands of weak to moderate intensity are exhibited by heteroaromatic compounds and their derivatives near to C-H vibrations of aromatic ring. Nature of the substituents does not affect the band appreciably in this

region. Symmetric mode of vibrations were observed with frequencies at 3192, 3195 and 3198 cm^{-1} in **1**, at 3181, 3194 and 3201 cm^{-1} in **2** and at 3193, 3194, 3195 and 3192 cm^{-1} in **3** respectively. Pure asymmetric stretching vibrations were computed at 3159, 3174 and 3175 cm^{-1} in **1**, at 3157 and 3164 cm^{-1} in **2** and at 3157, 3160, 3165, 3172 and 3175 cm^{-1} in **3** respectively. Mixed symmetric and asymmetric modes of vibrations were observed with wave numbers at 3184 and 3171 cm^{-1} in **1**, 3161, 3169, 3170 and 3182 cm^{-1} in **2** and 3169, 3182 and 3185 cm^{-1} in **3** respectively. In **1**, wave numbers computed at 1265, 1340 and 1598 cm^{-1} were assigned to rocking vibrations, 1265, 1655 cm^{-1} to scissoring vibrations and 755 cm^{-1} was assigned to wagging mode of vibration. Band observed at 831, 1106, 1495 cm^{-1} and 1595 cm^{-1} in **2** were due to the rocking and scissoring mode of vibrations respectively, while twisting vibrational band was computed at 805 cm^{-1}. Similarly in **3**, rocking vibrations were observed at 1489, 1496, 1543 cm^{-1}, scissoring vibrational bands at 1168, 1222 cm^{-1}, wagging mode of vibrations at 708, 764 cm^{-1} and twisting stretching modes were computed with vibrational bands at 805 and 829 cm^{-1} respectively (see Tables 5–7).

7.2. C-C stretching vibration

Generally, the C-C stretching modes of vibrations appear in the range of 1650–1400 cm^{-1} [43]. In our investigated compound (**1**), C-C vibrational bands were computed at 302, 583, 755, 1265, 1340, 1598 and 1655 cm^{-1} which are strongly supported by experimental calculated bands appeared at 312, 584, 752, 1267, 1354, 1698 and 1676 cm^{-1} respectively. Vibrational bands at 749, 1106, 1495 and 1596 cm^{-1} in **2** were observed due to C-C stretching mode of vibration and exhibit excellent agreement with experimental calculated bands with stretching frequencies 746, 1097, 1492 and 1593 cm^{-1} respectively. C-C stretching modes in **3** appeared at 780, 1168, 1222, 1489, 1496 and 1543 cm^{-1} shows good concurrence with experimental observed frequency at 786, 1168, 1224, 1489, 1506 and 1558 cm^{-1} respectively (see Tables 5–7).

7.3. Methyl group vibration

Methyl group C-H stretching vibrations are generally found in the region of 3000–2800 cm^{-1} [44]. In our studied compounds, methyl group is present only in **1** and **2**. Pure symmetric vibrational stretching modes were computed at 3033 and 3029 cm^{-1} in **1** and **2** respectively. Vibrational bands calculated at 3088, 3140 cm^{-1} in **1** and at 3120, 3129 in **2** were assigned to asymmetric vibrational stretching modes of methyl group C-H vibrations respectively (see Tables 5 and 6).

8. UV–Visible study

For chemical characterization of **1**, **2** and **3**, ultraviolet spectral analysis has been performed in gas phase using time-dependent DFT (TDDFT) calculations at B3LYP level of theory and 6-311 + G(2d,p) basis set combination to explain the charge transfer within the studied molecules, their absorption properties and vertical excitations. The results for TDDFT calculated absorption wavelengths (λ_{max}), excitation energy (E^{DFT}),

Table 8 Wave length, excitation energy and oscillator strength for **1, 2** and **3**.

Compounds	Cal. λ_{max} (nm)	E^{DFT} (eV)	f	MO contributions
1	340.84	3.6376	0.0006	H-2 → L(75%), H-2 → L + 1(15%),H-2 → L + 2(3%), H-2 → L + 3(2%)
	318.66	3.8909	0.3314	H → L(93%), H-1 → L(3%)
	307.04	4.6381	0.1100	H-1 → L(55%), H → L + 1(24%), H-3 → L(7%), H-3 → L + 1(3%),H → L(2%), H → L + 2 (2%)
	297.98	4.1608	0.0211	H-3 → L(69%),H-3 → L + 1(18%), H-1 → L(4%), H → L + 1(4%)
	280.82	4.4151	0.4263	H-1 → L(29%), H → L + 1(64%)
	274.99	4.5087	0.0107	H-4 → L(77%), H-1 → L + 2(2%), H → L + 2(6%), H → L + 3(7%)
2	347.83	3.5643	0.2391	H → L(96%)
	299.11	4.1449	0.1836	H → L + 1(54%), H-1 → L(28%), H-2 → L(7%), H-3→L(4%)
	293.64	4.2221	0.0115	H-3 → L(87%), H-3 → L + 1(2%), H → L + 1(6%)
	284.94	4.3509	0.1819	H-1 → L(56%), H → L + 1(19%), H → L + 2(12%), H-3→(4%)
	284.15	4.3631	0.0384	H-1 → L(10%), H → L + 2(74%), H-4 → L(6%), H-4 → L + 1(3%),
	274.33	4.51934	0.1951	H-2 → L(53%), H−1 →L + 1(26%), H → L + 1(15%)
3	326.61	3.7961	0.2316	H → L(91%)
	294.55	4.2093	0.0321	H-5 → L(2%), H-3 → L(42%), H-2 → L(29%), H → L(4%), H → L + 1(9%)
	291.49	4.2534	0.0174	H-3 → L(46%), H-2 → L(2%), H-1 → L(21%), H-1 → L + 1(3%), H → L + 1(22%)
	276.48	4.4844	0.1098	H-5 → L(4%), H-4 → L(3%), H-2 → L(3%), H-1 → L(13%), H → L + 1(11%), H → L + 2 (55%)
	275.66	4.4977	0.2541	H-6 → L(2.9%), H-2 → L(11.8%), H-1 → L(27%), H-1 → L + 1(2%), H → L + 1(18%), H → L + 2(27%)
	264.16	4.6936	0.3867	H-6 → L + 1(2%), H-5 → L(2%), H-2 → L(36%), H-1 → L + 1(15%), H → L + 1(30%), H → L + 3(6%)

E = Excitation energy (eV); λ = wave length (nm); f = oscillator strength; MO = molecular orbitals; H = HOMO, L = LUMO; λ (nm); Cal. = Calculated.

Table 9 Computed energies (E) for compounds **1**–**3**.

	1		2		3	
MO(s)	E (eV)	ΔE (eV)	E (eV)	ΔE (eV)	E (eV)	ΔE (eV)
HOMO	−6.594	4.273	−5.837	3.987	−6.087	4.263
LUMO	−2.321		−1.850		−1.824	
HOMO − 1	−7.007	5.254	−6.627	5.493	−6.672	5.584
LUMO + 1	−1.753		−1.134		−1.088	
HOMO−2	−7.165	6.246	−7.047	6.305	−6.988	6.047
LUMO + 2	−0.919		−0.742		−0.941	
HOMO − 3	−7.369	6.49	−7.180	6.877	−7.164	6.563
LUMO + 3	−0.879		−0.303		−0.601	

E = energy, ΔE (eV) = E_{LUMO}-E_{HOMO}; HOMO, highest occupied molecular orbital; LUMO, lowest unoccupied molecular orbital, MO, molecular orbital.

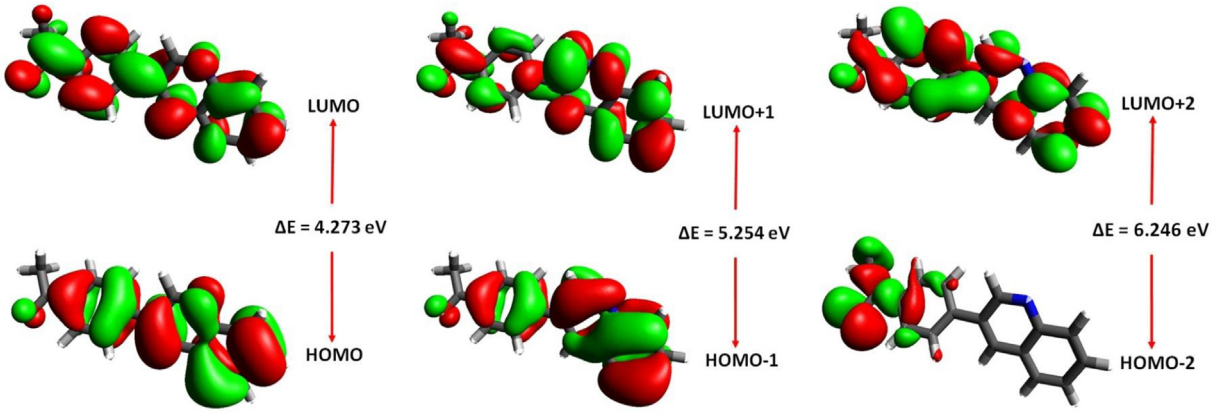

Fig. 4 Frontier molecular orbitals of **1**.

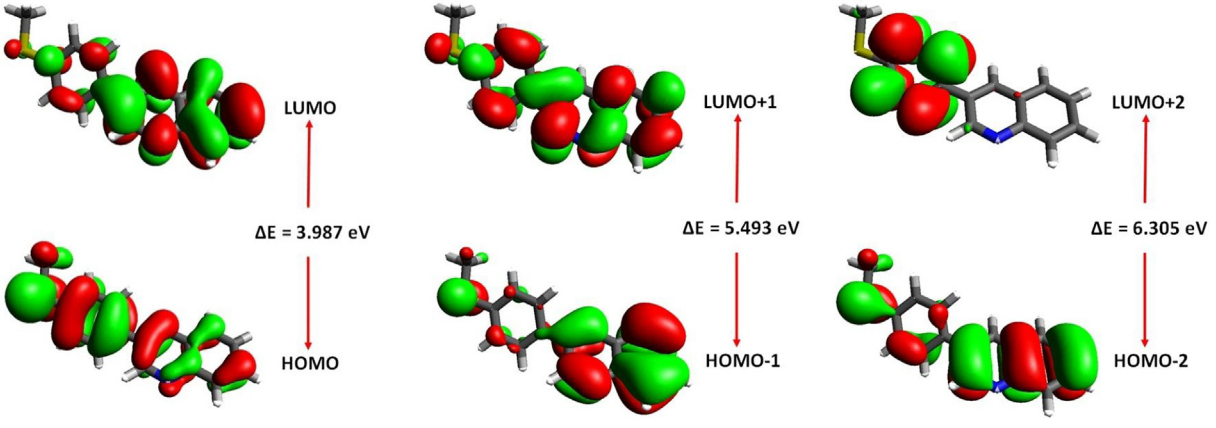

Fig. 5 Frontier molecular orbitals of **2**.

oscillator strength (f) and dominant molecular orbital contributions involved in **1**, **2** and **3** are presented in Table 8.

Results indicate that theoretically calculated main transition with maximum absorption values among all studied compounds is observed in **2** at 347.83 nm with E^{DFT}, f values of 3.5643, 0.2391 and main transition occurred from HOMO → LUMO (96%) respectively. The computed vertical excitation for **1** is mainly initiated from HOMO-2 → LUMO (75%) with λ_{max}, E^{DFT} and f value computed to be value of 340.84, 3.6376 and 0.0006 respectively. The absorption band with minimum absorption value among all studied compounds is observed in **3** at 326.61 nm with HOMO → LUMO (91%)

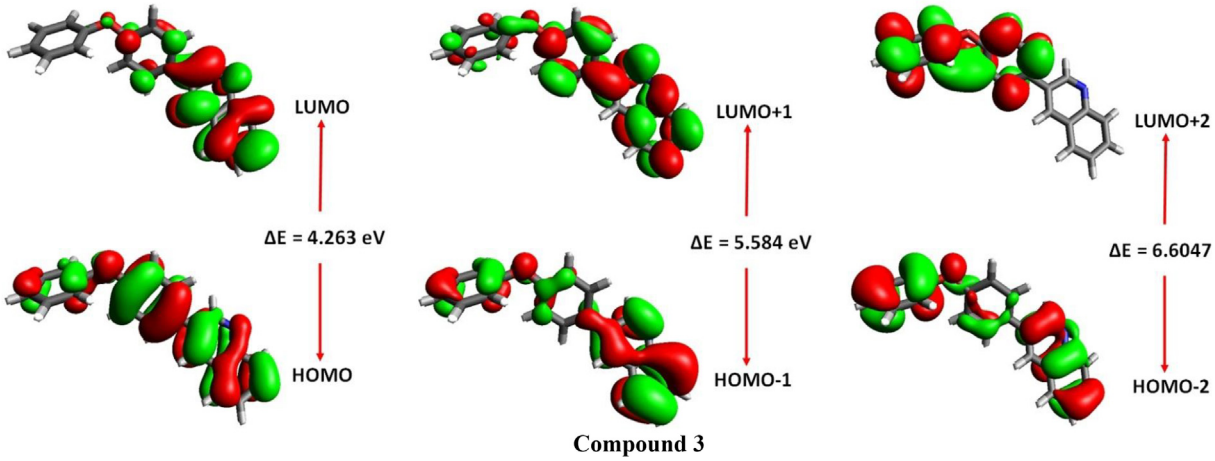

Fig. 6 Frontier molecular orbitals of **3**.

vertical excitation and 3.7961, 0.2316 values for E^{DFT} and *f* respectively. The incidence of absorption band with higher *f* and lower energy value as appeared in **2** is the characteristic of donor-acceptor molecules which is due to the complete intramolecular charge transfer and HOMO to LUMO electronic transitions. This results in red shift of absorption band in **2** as compared to **1** and **3**.

9. Frontier molecular orbital analysis

HOMO and LUMO collectively form frontier molecular orbitals (FMOs). HOMO term is used to describe the highest occupied molecular orbital having higher energy, rich numbers of electrons, therefore electron donating ability. Contrary, LUMO (lowest unoccupied molecular orbital) indicates the electron accepting capability due to lower energy and number deficiency of electrons. FMOs play a crucial role during molecular interactions. Furthermore, FMOs provide important perspective about the optical properties, electronic properties and reactivity of the molecule under investigation [17,18]. In this context, FMO analyses were carried out to predict the electronic properties of **1**, **2** and **3** at B3LYP level and 6311 + G (2d,p) basis set combination. Results of FMOs analysis consist of four important molecular orbital pairs, their gap energies (ΔE) and are presented in Table 9.

The least energy gap is found to be 3.987 eV in **2**, while highest energy gap value 4.273 eV is observed in **1.** The decreasing order of energy gap of studied compounds is:

1 > 3 > 2

The pictographic display of FMOs for **1**, **2** and **3** is presented in Figs. 4–6 respectively. Figs. 4–6 point out that HOMOs in **1**, **2** and **3** are populated over entire molecule. On the other hand, LUMOs in **1** are concentrated over all atoms and partially on quinoline ring in **2** and **3**.

Energies of HOMO, LUMO and their energy gaps are further used to describe the stability and reactivity of **1**, **2** and **3** by forecasting global reactivity descriptors [45–48]. Firstly, we calculated the electronic affinity (*A*) and ionization potential (*I*) in a vertical manner using Eqs. (2) and (3).

$$I = E_c^{N-1} - E_o^N \tag{2}$$

$$A = E_o^N - E_A^{N+1} \tag{3}$$

In Eqs. (1) and (2), I = Ionization potential; A = Electron affinity; E_c^{N-1} = cation (Energy after losing one electron); E_o^N = Basal state energy (neutral); E_A^{N+1} = anion (energy after gaining one electron). Hardness and electronegativity were obtained using Eqs. (4) and (5).

$$\eta = \frac{I - A}{2} \tag{4}$$

$$X = \frac{I + A}{2} \tag{5}$$

To establish the charge transfer process, electrophilicity calculations were performed which describe the relation among energy variation and maximum electron transferred.

$$\omega = \frac{\mu^2}{2\eta} \tag{6}$$

The donating or accepting ability of chemical species can be described with the help of two descriptors. The donating and accepting abilities of **1, 2** and **3** are calculated using Eqs. (7) and (8) respectively.

$$\omega^- = \frac{(3I + A)^2}{16\,(I - A)} \tag{7}$$

$$\omega^+ = \frac{(I + 3A)^2}{16(I - A)} \tag{8}$$

where ω^- = Electron donating capability; ω^+ = Electron accepting capability. The softness value is calculated using Eq. (9).

$$\sigma = \frac{1}{2\eta} \tag{9}$$

The results obtained from Eqs. (2)–(9) are presented in Table 10.

Maximum ionization potential is found to be 8.04 in **1**, while lowest ionization potential is observed in **2** with 7.28 values. The decreasing order of ionization potential is observed to be:

1 > 2 > 3

Table 10 Ionization potential (I), electron affinity (A), electronegativity (X), global hardness (η), chemical potential (μ), global electrophilicity (ω), electron donor capability (ω^-), electron acceptor capability (ω^+) and global softness (σ).

	I	A	X	η	μ	ω	ω-	ω+	σ
1	8.04	0.96	4.50	3.54	−4.50	2.86	5.55	1.05	0.14
2	7.28	0.41	3.84	3.43	−3.84	2.15	4.50	0.65	0.14
3	7.41	0.40	3.90	3.50	−3.90	2.17	4.57	0.66	0.14

A highest electron affinity value is found to be 0.96 in **1**. 0.40 is the least value of electron affinity observed in **3**. Since ionization potential and electron affinity values are used to describe the electron releasing and accepting capability of molecules under investigation which are directly related to the energy of HOMOs and LUMOs. Therefore, it is evident in our studied systems too where order of ionization potential and electron affinity exactly matches with energy of HOMOs and LUMOs respectively. Overall, ionization potential values are observed larger as compared to electron affinity values describing the better electron donating capability of studied molecules. Normally, a molecule with high energy gap is considered to be hard, non-reactive, stable and vice versa. This postulate also holds in our studied systems where global hardness values are found exactly in order of energy gap order **1** > **3** > **2.**

Compound (**1**) contains the highest energy gap and global hardness values. Similarly, **2** holds the least energy gap and smallest hardness values among all studied compounds. A similar trend is observed in case of electronegativity values of studied compounds. Highest electronegativity value (4.50) is found to be in **1**, while lowest (3.84) is observed in **2**. Value of chemical potential is used to describe the reactivity and stability of the molecules under investigation. Molecules with greater chemical potential values are considered less reactive, more stable and vice versa. The increasing order of chemical potential for all four compounds is:

$$[\mathbf{1}(\mu = -4.50\,\text{eV})] < [\mathbf{3}(\mu = -3.90\,\text{eV})] < [\mathbf{2}(\mu = -3.84\,\text{eV})].$$

Global softness value of all studied compounds is found to be same with 0.14 eV. These values are found 25.28, 24.5 and 25 times less than their respective global hardness values respectively. The global electrophilicity (ω), electron donor capability (ω^-) and electron acceptor capability (ω^+) of all studied compounds are also found in the following decreasing order: **1** > **3** > **2.**

Overall, the electron donating capability values are found greater in magnitude as compared to electron accepting capability values. Since ionization potential and electron affinity values represent the electron donating and accepting abilities respectively. In our investigated systems, ionization potential values are found much higher than their electron affinity values which strengthen the findings of greater electron donor capability (ω^-) of investigated compounds as compared to electron acceptor capability (ω^+). The preceding results indicate that all investigated molecules are chemically hard compounds with greater kinetic stability and electron donating capability.

10. Nonlinear optical (NLO) properties

Exploration of NLO properties of organic materials is the hot area of research recently. Due to ultrafast electronic responses and less dielectric constants, organic NLO materials are getting impressive consideration in various optoelectronic applications. Presence of large delocalization of electrons and intramolecular charge transfer (ICT) in organic materials extend their uses to optical fiber telecommunication sector. NLO character instigates due to non-centrosymmetric nature and architecture of the molecules. This can be achieved by positioning of appropriate donor-acceptor units and alteration of π-conjugation length [49–51]. NLO properties of **1, 2** and **3** are investigated in combination of B3LYP level of theory and 6311 + G(2d,p) basis set. Average polarizability (α) is estimated by considering the diagonal elements of the Eq. (10).

$$\langle\alpha\rangle = 1/3(\alpha_{xx} + \alpha_{yy} + \alpha_{zz}) \tag{10}$$

First hyperpolarizability (β_{tot}) and second hyperpolarizability $\langle\gamma\rangle$ are calculated using following Eqs. (11) and (12) by considering the x, y and z-direction tensors.

$$\beta_{tot} = \left[\left(\beta_{xxx} + \beta_{xyy} + \beta_{xzz}\right)^2 + \left(\beta_{yyy} + \beta_{xxy} + \beta_{yzz}\right)^2 + \left(\beta_{zzz} + \beta_{xxz} + \beta_{yyz}\right)^2\right]^{1/2} \tag{11}$$

$$\langle\Upsilon\rangle = \frac{1}{5}\left(\Upsilon_{xxxx} + \Upsilon_{yyyy} + \Upsilon_{zzzz} + 2\left[\Upsilon_{xxyy} + \Upsilon_{yyzz} + \Upsilon_{xxzz}\right]\right) \tag{12}$$

The calculated results for dipole moments and linear polarizabilities of **1**, **2** and **3** are depicted in Table 11, while results of first hyperpolarizability (second order NLO; β_{tot}) and second hyperpolarizability are presented in Tables 12 and 13 correspondingly. In our studied molecules, comparative study of dipole moment describes the distribution of charges in different directions. Compound (**2**) with a dipole moment value of 3.2980 D is the largest computed dipole moment among all

Table 11 The dipole moment (D) and computed dipole polarizabilities for **1**, **2** and **3.**

	μ_x	μ_y	μ_z	μ	α_{xx}	α_{yy}	α_{zz}	α_{total} (a.u)
1	−1.6125	0.4826	1.4421	2.2165	389.65	195.59	118.89	234.71
2	−1.2024	3.0710	−0.0186	3.2980	408.60	201.41	124.87	244.96
3	1.6579	2.7101	0.1736	3.1817	441.72	246.26	159.46	282.48

Table 12 The computed first hyperpolarizability/second order NLO (a.u.) for **1**, **2** and **3.**

	β_{xxx}	β_{xxy}	β_{xyy}	β_{yyy}	β_{xxz}	β_{yyz}	β_{xzz}	β_{yzz}	β_{zzz}	β_{tot} (a.u)
1	2315.14	−146.415	−76.5478	46.8009	19.1004	−4.25875	−74.8029	6.74514	48.7214	2166.71
2	2967.12	−14.9805	−5.75494	4.94261	−10.7179	15.8083	−1.56733	9.74826	−41.1794	2960.02
3	−1770.49	372.634	25.8754	72.6179	−47.3759	−20.9111	−19.8578	38.7229	2.10436	1830.84

Table 13 The second hyperpolarizability values for **1**, **2** and **3.**

	γ_{xxxx}	γ_{yyyy}	γ_{zzzz}	γ_{xxzz}	γ_{zzxx}	γ_{yyzz}	$\langle\gamma\rangle$ (a.u.)
1	−9109.32	−931.403	−240.621	−1773.75	−1665.04	−198.216	−11736.1
2	−8656.66	−961.258	−246.156	−1700.97	−1764.68	−205.358	−11332.4
3	−13968.7	−1423.842	−399.146	−2681.42	−2681.85	−309.810	−18060.9

studied compounds. Lowest value of computed dipole moment is found to be 2.2165 D in **1**. Overall, dipole moment is found to be in following decreasing order: **2** > **3** > **1**.

In literature, urea molecule is widely found as a standard for comparison of dipole moment and first hyperpolarizability values. Dipole moment of all molecules is found to be greater than the urea molecule dipole moment (1.3732 D) [52]. Compounds **1**, **2** and **3** are found to be with 1.61, 2.40 and 2.32 times greater than the urea molecule dipole moment value respectively. In case of linear polarizability, the results of polarizability tensors along x, y and z directions indicate that x-axis polarizability tensor is dominant among all tensors and contributed well in total linear polarizability values. Among all studied compounds, compound with largest linear polarizability value is **3** with total dipole polarizability value of 282.48 a.u. On the other hand, least dipole polarizability value 234.71 a.u is noticed in **1**. The decreasing order of total linear polarizability value is: **3** > **2** > **1**.

The values of β_{tot} along with its nine contributing tensors along x, y, and z-directions are presented in Table 12. Results reveal that transition which made dominant contribution for calculation of β_{tot} are found along x-axis direction with positive value in **1–2** and negative value in **3.** Highest β_{tot} value among **1–3** is observed to be with 2960.02 (a.u) value in **2**. This highest value results due to the highest contribution of x-axis transition among three compounds. On the other hand, least value of β_{tot} is noticed 1830.84 (a.u) in **3** due to least contribution of dominant x-axis transition among three investigated compounds. The order of β_{tot} for investigated compounds **1–3** is found to be in following decreasing order: **2** > **1** > **3.** For comparative NLO analysis, we further compared our results with reference urea molecule urea molecule (β_{tot} (urea) = 43 a.u) [52]. The β_{tot} values of all compounds are found greater than the urea molecule. The β_{tot} values of **1**, **2** and **3** are computed 50.39, 68.84 and 42.58 times greater than the urea molecule respectively.

The second hyperpolarizability values along x direction are found to be −9109.32 a.u. −8656.66 a.u. and −13968.7 a.u. in **1**, **2** and **3** respectively, which are larger than their y and z directions hyperpolarizability tensors (see Table 13). Total second hyperpolarizability value is found to be maximum −11332.4 a.u. in **2**, while lowest with −18060.9 a.u. value in **3**. The decreasing order of β_{tot} observed in investigated compounds is: **2** > **1** > **3.**

On the basis of the complex sum-over-states (SOS) expression, two-state model was formulated by Oudar and Chemla [53] which has been exercised in our study to further reinforce our NLO results. The expression for this model is represented in Eq. (13) which describes the relation between first hyperpolarizability value and charge transfer transitions.

$$\beta = \frac{\Delta\mu_{gm} f_{gm}}{E_{gm}^3} \tag{13}$$

From this equation, it can be seen that there is a direct relation of first hyperpolarizability (β) with product of ground state-excited state transition moment ($\Delta\mu_{gm}$) and oscillator strength (f_{gm}); while inverse relation with cube of the transition energy (E_{gm}^3). From Eq. (13), it is evident that the large f_{gm} value and small (E_{gm}^3) results in large β value. The values of f_{gm} and E_{gm}^3 for **1**, **2** and **3** are given in Table 8. Due to same general architecture of compounds **1–3**, there is not much difference in the transition dipole moment, thus considered as constant. The value of f_{gm} for investigated compounds is also found almost same. Therefore, only E_{gm}^3 is the decisive factor for the determination of β value. E_{gm}^3 values of **1**, **2** and **3** is found to be 3.6376, 3.5643 and 3.7961 eV respectively, which results in larger β value of **2** and smaller β value of **3**. The order of E_{gm}^3 (**2** < **1** < **3**) correspond nicely with the reverse order of β (**2** > **1** > **3**). Thus, two–state model also validate the conclusion of larger NLO response of investigated compounds. In a nutshell, urea molecule comparative analysis and two-state model proposed that investigated molecules are excellent NLO candidates and may have prospective uses in the technology related applications.

11. Conclusions

In the present study, we report the synthesis of three novel arylated quinolines derivatives **1**, **2** and **3** employing Pd catalyzed Suzuki–Miyaura cross-coupling reaction. The chemical structures of all compounds were resolved employing different analytical techniques like ^{1}H-NMR, FT-IR, UV–Vis, EIMS,

elemental analysis and finally confirmed by single crystal X-ray diffraction analysis. The crystal structures of all studied compounds exhibited monoclinic shape with P21/c space groups. Geometrical parameters (bond length and bond angles) of all compounds obtained from crystal structures are agreed well with the DFT optimized geometric parameters. The experimental FT-IR spectra were also well reproduced by the DFT calculations. The UV–Vis analysis indicated the red shift of absorption band in **2** as compared to **1**, **3** and reveal the occurrence of maximum excitations from $\pi \rightarrow \pi^*$ excitations. NBO calculation indicated the occurrence of intra-molecular charge transfer in all compounds, hence enormous molecular stability owing to hyperconjugative interactions. The energies of HOMO and LUMO were utilized to examine the charge transfer. Energy of FMO was used to calculate global reactivity descriptors which indicate that synthesized molecules are chemically hard compounds with greater kinetic stability and electron donating capability. Global hardness values of all compounds were found to be 25 times greater than respective global softness value. NLO properties were found to be in the range 1830–2960 a.u and order of **2** > **1** > **3.** Urea molecule comparative analysis and two-state model confirmed that synthesized molecules are excellent NLO candidates and may have prospective uses in the technology related applications.

Acknowledgments

Ataualpa A.C. Braga acknowledges financial support by Fundação de Amparo à Pesquisa do Estado de São Paulo (2015/01491-3 and 2014/25770-6).

Appendix A. Supplementary data

Supplementary data to this article can be found online at https://doi.org/10.1016/j.jscs.2018.09.006.

References

[1] K. Majerz-Maniecka, B. Oleksyn, R. Musiol, B. Podeszwa, J. Polanski, Joint meeting on medicinal chemistry. Vienna, Austria, June 20–23, Sci. Pharm. 73(Suppl 1) (2005) 194.
[2] S.J. Benkovic, S.J. Baker, M. Alley, Y.-H. Woo, Y.-K. Zhang, T. Akama, W. Mao, J. Baboval, P.R. Rajagopalan, M. Wall, Identification of borinic esters as inhibitors of bacterial cell growth and bacterial methyltransferases, CcrM and MenH, J. Med. Chem. 48 (23) (2005) 7468–7476.
[3] S.Y. Ablordeppey, P. Fan, S. Li, A.M. Clark, C.D. Hufford, Substituted indoloquinolines as new antifungal agents, Biorg. Med. Chem. 10 (5) (2002) 1337–1346.
[4] O. Afzal, S. Kumar, M.R. Haider, M.R. Ali, R. Kumar, M. Jaggi, S. Bawa, A review on anticancer potential of bioactive heterocycle quinoline, Eur. J. Med. Chem. 97 (2015) 871–910.
[5] S.A. Jenekhe, L. Lu, M.M. Alam, New conjugated polymers with donor–acceptor architectures: synthesis and photophysics of carbazole–quinoline and phenothiazine–quinoline copolymers and oligomers exhibiting large intramolecular charge transfer, Macromolecules 34 (21) (2001) 7315–7324.
[6] Y.-L. Zhao, Y.-L. Chen, F.-S. Chang, C.-C. Tzeng, Synthesis and cytotoxic evaluation of certain 4-anilino-2-phenylquinoline derivatives, Eur. J. Med. Chem. 40 (8) (2005) 792–797.
[7] Y.-L. Chen, C.-J. Huang, Z.-Y. Huang, C.-H. Tseng, F.-S. Chang, S.-H. Yang, S.-R. Lin, C.-C. Tzeng, Synthesis and antiproliferative evaluation of certain 4-anilino-8-methoxy-2-phenylquinoline and 4-anilino-8-hydroxy-2-phenylquinoline derivatives, Biorg. Med. Chem. 14 (9) (2006) 3098–3105.
[8] B. Joseph, F. Darro, A. Béhard, B. Lesur, F. Collignon, C. Decaestecker, A. Frydman, G. Guillaumet, R. Kiss, 3-Aryl-2-quinolone derivatives: synthesis and characterization of in vitro and in vivo antitumor effects with emphasis on a new therapeutical target connected with cell migration, J. Med. Chem. 45 (12) (2002) 2543–2555.
[9] D. Edmont, R. Rocher, C. Plisson, J. Chenault, Synthesis and evaluation of quinoline carboxyguanidines as antidiabetic agents, Bioorg. Med. Chem. Lett. 10 (16) (2000) 1831–1834.
[10] D.G. Batt, J.J. Petraitis, S.R. Sherk, R.A. Copeland, R.L. Dowling, T.L. Taylor, E.A. Jones, R.L. Magolda, B.D. Jaffee, Heteroatom-and carbon-linked biphenyl analogs of Brequinar as immunosuppressive agents, Bioorg. Med. Chem. Lett. 8 (13) (1998) 1745–1750.
[11] C. Papageorgiou, A. von Matt, J. Joergensen, E. Andersen, K. Wagner, C. Beerli, T. Than, X. Borer, A. Florineth, G. Rihs, Aromatic quinolinecarboxamides as selective, orally active antibody production inhibitors for prevention of acute xenograft rejection, J. Med. Chem. 44 (12) (2001) 1986–1992.
[12] D. Narsinh, S. Anamik, Synthesis and anti-HIV studies of some substituted pyrimidinediones, ethoxy pyrano (3, 2-c) quinolines and hydrazino pyrano (3, 2-c) quinolines, Ind. J. Pharm. Sci. 63 (2001) 211–215.
[13] R.D. Dillard, D.E. Pavey, D.N. Benslay, Synthesis and antiinflammatory activity of some 2, 2-dimethyl-1, 2-dihydroquinolines, J. Med. Chem. 16 (3) (1973) 251–253.
[14] M. Sechi, G. Rizzi, A. Bacchi, M. Carcelli, D. Rogolino, N. Pala, T.W. Sanchez, L. Taheri, R. Dayam, N. Neamati, Design and synthesis of novel dihydroquinoline-3-carboxylic acids as HIV-1 integrase inhibitors, Biorg. Med. Chem. 17 (7) (2009) 2925–2935.
[15] D. Dubé, M. Blouin, C. Brideau, C.-C. Chan, S. Desmarais, D. Ethier, J.-P. Falgueyret, R.W. Friesen, M. Girard, Y. Girard, Quinolines as potent 5-lipoxygenase inhibitors: synthesis and biological profile of L-746,530, Bioorg. Med. Chem. Lett. 8 (10) (1998) 1255–1260.
[16] H. Shinkai, T. Ito, T. Iida, Y. Kitao, H. Yamada, I. Uchida, 4-Aminoquinolines: novel nociceptin antagonists with analgesic activity, J. Med. Chem. 43 (24) (2000) 4667–4677.
[17] C.H. Kaschula, T.J. Egan, R. Hunter, N. Basilico, S. Parapini, D. Taramelli, E. Pasini, D. Monti, Structure–activity relationships in 4-aminoquinoline antiplasmodials. The role of the group at the 7-position, J. Med. Chem. 45 (16) (2002) 3531–3539.
[18] N. Muruganantham, R. Sivakumar, N. Anbalagan, V. Gunasekaran, J.T. Leonard, Synthesis, anticonvulsant and antihypertensive activities of 8-substituted quinoline derivatives, Biol. Pharm. Bull. 27 (10) (2004) 1683–1687.
[19] B.S. Holla, M. Mahalinga, M.S. Karthikeyan, P.M. Akberali, N.S. Shetty, Synthesis of some novel pyrazolo [3, 4-d] pyrimidine derivatives as potential antimicrobial agents, Biorg. Med. Chem. 14 (6) (2006) 2040–2047.
[20] X. Zhang, S.A. Jenekhe, Electroluminescence of multicomponent conjugated polymers. 1. Roles of polymer/polymer interfaces in emission enhancement and voltage-tunable multicolor emission in semiconducting polymer/polymer heterojunctions, Macromolecules 33 (6) (2000) 2069–2082.
[21] M.-H. Kim, J.-I. Jin, C.-J. Lee, N.-J. Kim, K.-H. Park, Synthesis and characterization of nonlinear optical polymers having quinoline-based chromophores, Bull. Korean Chem. Soc. 23 (7) (2002) 964–970.
[22] A. Farag, N. Roushdy, S.A. Halim, N.M. El-Gohary, M.A. Ibrahim, S. Said, Synthesis, molecular, electronic structure, linear and non-linear optical and phototransient properties of 8-methyl-1, 2-dihydro-4H-chromeno [2, 3-b] quinoline-4, 6 (3H)-dione (MDCQD): Experimental and DFT investigations,

Spectrochim. Acta. A Mol. Biomol. Spectrosc. 191 (2018) 478–490.
[23] G.W. Ejuh, N. Samuel, T.N. Fridolin, N.J. Marie, Computational determination of the electronic and nonlinear optical properties of the molecules 2-(4-aminophenyl) quinoline, 4-(4-aminophenyl) quinoline, anthracene, anthraquinone and phenanthrene, Mater. Lett. 178 (2016) 221–226.
[24] M.A. Ullah, M. Adeel, M.N. Tahir, I. Ullah, M. Raza, Synthesis and single crystal X-ray studies of 3-(3, 5-bis (trifluoromethyl) phenyl) quinoline and 3-(4-fluoro-3-methylphenyl) quinoline, Chin. J. Struc. Chem. 33 (1) (2013) 90–96.
[25] A.U. Malik, M. Adeel, I. Ullah, M.K. Baloch, M. Mustaqeem, M. Akram, Solubility of 3-{3, 5-Bis (trifluoromethyl) phenyl} quinoline Using Micellar Solutions of Surfactants, J. Solution Chem. 44 (6) (2015) 1191–1204.
[26] M.A. Ullah, M. Adeel, M.N. Tahir, A. Rauf, M. Akram, T.B. Hadda, Y.N. Mabkhot, N. Muhammad, F. Naseer, M.S. Mubarak, Synthesis, structural characterization and antinociceptive activities of new arylated quinolines via Suzuki-Miyaura cross coupling reaction, Medicinal Chem. 13 (8) (2017) 780–786.
[27] M. Shahid, M. Salim, M. Khalid, M.N. Tahir, M.U. Khan, A. A.C. Braga, Synthetic, XRD, non-covalent interactions and solvent dependent nonlinear optical studies of Sulfadiazine-Ortho-Vanillin Schiff base:(E)-4-((2-hydroxy-3-methoxy-benzylidene) amino)-N-(pyrimidin-2-yl) benzene-sulfonamide, J. Mol. Struct. 1161 (2018) 66–75.
[28] M. Adeel, A.A. Braga, M.N. Tahir, F. Haq, M. Khalid, M.A. Halim, Synthesis, X-ray crystallographic, spectroscopic and computational studies of aminothiazole derivatives, J. Mol. Struct. 1131 (2017) 136–148.
[29] S. Naseem, M. Khalid, M.N. Tahir, M.A. Halim, A.A. Braga, M.M. Naseer, Z. Shafiq, Synthesis, structural, DFT studies, docking and antibacterial activity of a xanthene based hydrazone ligand, J. Mol. Struct. 1143 (2017) 235–244.
[30] M.N. Arshad, A.-A.M. Al-Dies, A.M. Asiri, M. Khalid, A.S. Birinji, K.A. Al-Amry, A.A. Braga, Synthesis, crystal structures, spectroscopic and nonlinear optical properties of chalcone derivatives: a combined experimental and theoretical study, J. Mol. Struct. 1141 (2017) 142–156.
[31] M.S. Ahmad, M. Khalid, M.A. Shaheen, M.N. Tahir, M.U. Khan, A.A.C. Braga, H.A. Shad, Synthesis and XRD, FT-IR vibrational, UV–vis, and nonlinear optical exploration of novel tetra substituted imidazole derivatives: a synergistic experimental-computational analysis, J. Phys. Chem Solids (2017).
[32] M.N. Tahir, M. Khalid, A. Islam, S.M.A. Mashhadi, A.A. Braga, Facile synthesis, single crystal analysis, and computational studies of sulfanilamide derivatives, J. Mol. Struct. 1127 (2017) 766–776.
[33] M. Akram, M. Adeel, M. Khalid, M.N. Tahir, M.U. Khan, M. A. Asghar, M.A. Ullah, M. Iqbal, A combined experimental and computational study of 3-bromo-5-(2, 5-difluorophenyl) pyridine and 3, 5-bis (naphthalen-1-yl) pyridine: Insight into the synthesis, spectroscopic, single crystal XRD, electronic, nonlinear optical and biological properties, J. Mol. Struct. 1160 (2018) 129–141.
[34] A.A. Braga, G. Ujaque, F. Maseras, A DFT study of the full catalytic cycle of the Suzuki-Miyaura cross-coupling on a model system, Organometallics 25 (15) (2006) 3647–3658.
[35] M. García-Melchor, A.A. Braga, A. Lledós, G. Ujaque, F. Maseras, Computational perspective on Pd-catalyzed C-C cross-coupling reaction mechanisms, Acc. Chem. Res. 46 (11) (2013) 2626–2634.
[36] A.A. Braga, N.H. Morgon, G. Ujaque, F. Maseras, Computational characterization of the role of the base in the Suzuki-Miyaura cross-coupling reaction, J. Am. Chem. Soc. 127 (25) (2005) 9298–9307.
[37] M.J. Frisch, G.W. Trucks, H.B. Schlegel, G. Scuseria, M.A. Robb, J.R. Cheeseman, G. Scalmani, V. Barone, B. Mennucci, G. Petersson, H. Nakatsuji, M. Caricato, X. Li, H.P. Hratchian, A.F. Izmaylov, J. Bloino, G. Zheng, J.L. Sonnenberg, M. Hada, M. Ehara, K. Toyota, R. Fukuda, J. Hasegawa, M. Ishida, T. Nakajima, Y. Honda, O. Kitao, H. Nakai, T. Vreven, J.A. Montgomery, J.E. Peralta, F. Ogliaro, M. Bearpark, J.J. Heyd, E. Brothers, K.N. Kudin, V.N. Staroverov, R. Kobayashi, J. Normand, K. Raghavachari, A. Rendell, J.C. Burant, S.S. Iyengar, J. Tomasi, M. Cossi, N. Rega, J.M. Millam, M. Klene, J.E. Knox, J.B. Cross, V. Bakken, C. Adamo, J. Jaramillo, R. Gomperts, R.E. Stratmann, O. Yazyev, A.J. Austin, R. Cammi, C. Pomelli, J.W. Ochterski, R.L. Martin, K. Morokuma, V.J. Zakrzewski, G.A. Voth, P. Salvador, J.J. Dannenberg, S. Dapprich, A.D. Daniels, O. Farkas, J.B. Foresman, J.V. Ortiz, J. Cioslowski, D.J. Fox, D. 0109, Revision D. 01, Gaussian, Inc., Wallingford, CT, 2009.
[38] R. Dennington, T. Keith, J. Millam, GaussView, version 5, Semichem Inc., Shawnee Mission, KS, 2009.
[39] Avagadro, http://avogadro.cc/wiki/Main_Page.
[40] ChemCraft, http://www.chemcraftprog.com.
[41] E.D. Glendening, C.R. Landis, F. Weinhold, Natural bond orbital methods, Wiley Interdisciplinary Rev.: Comput. Mol. Sci. 2 (1) (2012) 1–42.
[42] G. Socrates, Infrared and Raman characteristic group frequencies: table and charts, Ltd WJS (2001) 1–347.
[43] D. Sathiyanarayanan, Vibrational Spectroscopy Theory and Application, New Age International Publishers, New Delhi, 2004.
[44] R. Lu, W. Gan, B.-H. Wu, Z. Zhang, Y. Guo, H.-F. Wang, C–H stretching vibrations of methyl, methylene and methine groups at the vapor/alcohol (n = 1–8) interfaces, J. Phys. Chem. B 109 (29) (2005) 14118–14129.
[45] R.G. Parr, L.V. Szentpaly, S. Liu, Electrophilicity index, J. Am. Chem. Soc 121 (9) (1999) 1922–1924.
[46] R.G. Parr, R.A. Donnelly, M. Levy, W.E. Palke, Electronegativity: the density functional viewpoint, J. Chem. Phys. 68 (8) (1978) 3801–3807.
[47] P.K. Chattaraj, U. Sarkar, D.R. Roy, Electrophilicity index, Chem. Rev. 106 (6) (2006) 2065–2091.
[48] A. Lesar, I. Milošev, Density functional study of the corrosion inhibition properties of 1, 2, 4-triazole and its amino derivatives, Chem. Phys. Lett. 483 (4) (2009) 198–203.
[49] M.U. Khan, M. Khalid, M. Ibrahim, A.A.C. Braga, M. Safdar, A.A. Al-Saadi, M.R.S.A. Janjua, First Theoretical framework of triphenylamine–dicyanovinylene-based nonlinear optical dyes: structural modification of π-linkers, J. Phys. Chem. C 122 (7) (2018) 4009–4018.
[50] M.R.S.A. Janjua, M.U. Khan, B. Bashir, M.A. Iqbal, Y. Song, S.A.R. Naqvi, Z.A. Khan, Effect of π-conjugation spacer (C C) on the first hyperpolarizabilities of polymeric chain containing polyoxometalate cluster as a side-chain pendant: a DFT study, Comp. Theor. Chem. 994 (2012) 34–40.
[51] M.R.S.A. Janjua, M. Amin, M. Ali, B. Bashir, M.U. Khan, M. A. Iqbal, W. Guan, L. Yan, Z.M. Su, A DFT study on the two-dimensional second-order Nonlinear Optical (NLO) response of terpyridine-substituted hexamolybdates: physical insight on 2D inorganic-organic hybrid functional materials, Eur. J. Inorg. Chem. 2012 (4) (2012) 705–711.
[52] P.N. Prasad, D.J. Williams, Introduction to Nonlinear Optical Effects in Molecules and Polymers, Wiley, New York, 1991, etc.
[53] J.-L. Oudar, D. Chemla, Hyperpolarizabilities of the nitroanilines and their relations to the excited state dipole moment, J. Chem. Phys. 66 (6) (1977) 2664–2668.